Detection of Driver Vigilance Level Using EEG Signals and Driving Contexts

Zizheng Guo, Yufan Pan, Guozhen Zhao, Shi Cao, and Jun Zhang

***Abstract*—Quantitative estimation of a driver's vigilance level has a great value for improving driving safety and preventing accidents. Previous studies have identified correlations between electroencephalogram (EEG) spectrum power and a driver's mental states such as vigilance and alertness. Studies have also built classification models that can estimate vigilance state changes based on data collected from drivers. In the present study, we propose a system to detect vigilance level using not only a driver's EEG signals but also driving contexts as inputs. We combined a support vector machine with particle swarm optimization methods to improve classification accuracy. A simulated driving task was conducted to demonstrate the reliability of the proposed system. Twenty participants were assigned a 2-h sustained-attention driving task to identify a lead car's brake events. Our system was able to account for 84.1% of experimental reaction times with 162-ms prediction errors. A newly introduced driving context factor, road curves, improved the prediction accuracy by 2–5% with 30–80 ms smaller errors. These findings demonstrated the potential value of the proposed system for estimating driver vigilance level on a time scale of seconds.**

***Index Terms*—Driver vigilance, driving context, driving safety, electroencephalogram (EEG), support vector machine (SVM).**

NOMENCLATURE

Acronyms and abbreviations

RT	Reaction time.
SVM	Support vector machine.
EEG	Electroencephalogram.
PSD	Power spectral density.
EMG	Electromyography.
ICA	Independent component analysis.
EOG	Electrooculography.
STFT	Short-time Fourier transform.
FFT	Fast Fourier transform.
SVR	Support vector regression.
LSSVM	Least-squares support vector machine.
RBF	Radial basis function.
PSO	Particle swarm optimization.
RMSE	Root-mean-square error.

Notations

m	Number of epochs.
PSD_i	PSD extracted from the ith epoch.
w	Weight vectors of the PSD features.
r	Road condition.
X	EEG and driving context feature vectors.
Y	Regression goal vectors.
l	Number of training data.
ω	Optimal hyperplane.
ξ, ξ^*	Slack variables of SVR.
C	Constant to adjust SVR to avoid overfitting or underfitting.
$k(\cdot)$	Kernel function.
σ	Width of the RBF.
W	Weight vectors of training data in LSSVM.
d	Bias.
$\phi(\cdot)$	Function mapping to the high dimensional feature space.
ε	Error vector.
α	Lagrange multiplier.
t	tth generation of PSO.
c_1, c_2	Learning factors.
$v_{n,d}^t$	Velocity of particle n in dimension d for the tth generation.
$p_{n,d}^t$	Position of the particle n in dimension d for the tth generation.
$P_{l\mathrm{best}}, P_{g\mathrm{best}}$	Local best position and the global best position.
r_1, r_2	Normally distributed random numbers between 0 and 1.
η	Constraint factor of velocity.
ϖ	Inertial weight coefficient $v_{n,d}^t$.

Manuscript received January 19, 2017; revised July 13, 2017 and October 30, 2017; accepted November 24, 2017. Date of publication December 27, 2017; date of current version March 1, 2018. This work was supported in part by the National Key Research and Development Plan under Grant 2016YFB1001200 and in part by the National Natural Science Foundation of China under Grant 51108390 and Grant 31771226. Associate Editor: S. Li. *(Corresponding author: Guozhen Zhao.)*

Z. Guo was with the Key Laboratory of Behavioral Science, Institute of Psychology, Chinese Academy Sciences, Beijing 100101, China. He is now with the School of Transportation and Logistics, Southwest Jiaotong University, Chengdu 610031, China (e-mail: guozizheng@swjtu.edu.cn).

Y. Pan and J. Zhang are with the School of Transportation and Logistics, Southwest Jiaotong University, Chengdu 610031, China (e-mail: pyf066@my.swjtu.edu.cn; zhangjun@swjtu.edu.cn).

G. Zhao is with the Key Laboratory of Behavioral Science, Institute of Psychology, Chinese Academy Sciences, Beijing 100101, China (e-mail: zhaogz@psych.ac.cn).

S. Cao is with the Department of Systems Design Engineering, University of Waterloo, Waterloo, ON N2L 3G1, Canada (e-mail: shi.cao@uwaterloo.ca).

Color versions of one or more of the figures in this paper are available online at http://ieeexplore.ieee.org.

Digital Object Identifier 10.1109/TR.2017.2778754

I. INTRODUCTION

MANY tasks such as driving a car require human operators to be vigilant. Vigilance is a term with varied definitions, but the most common usage is sustained attention or tonic alertness, an ability to sustain attention to a task for

0018-9529 © 2017 IEEE. Translations and content mining are permitted for academic research only. Personal use is also permitted, but republication/redistribution requires IEEE permission. See http://www.ieee.org/publications_standards/publications/rights/index.html for more information.

a period of time [1]. Long-term and monotonous driving often lead to the decrease of vigilance levels [2], [3], which is one of the major factors causing traffic accidents. Statistics show that approximately 10–20% of road traffic accidents are due to drivers' decreased vigilance levels [4], [5]. Therefore, it is important to develop a system to monitor driver vigilance level and make appropriate interventions when declining vigilance is detected. A straightforward solution is to give an auditory warning signal to the driver when his vigilance level is predicted to decline. With such a vigilance monitoring system, drivers respond more quickly and safely to an immediate road event (e.g., a lead car brakes suddenly) [6]. A more sophisticated system based on driver vigilance detection is a vehicle active safety model to control parameters such as vehicle speed and to invoke automatic braking in an emergency [7].

Over the years, researchers have made great progress in developing vigilance detection systems. The most reliable systems can be classified into two categories according to the types of their input signals. One category analyzes an individual's driving performance to evaluate the level of vigilance. For example, vigilance is measured as the RT from the onset of a stimulus (e.g., brake lights of a lead car) to a driver's response (e.g., pressing a button). Longer RT indicates lower vigilance. Similar measures include lane deviation from the central line, steering wheel angle, and accelerator pedal position. Zhao *et al.* [8] studied the reliability of steering behavior to detect a driver's vigilance level using a multiwavelet packet energy spectrum with SVM techniques. They judged the level of vigilance by relying on the RT to a changed line signal. The best system performance (i.e., the fit of classification model predictions to experimental data) reached 95%. In another study conducted by Liu and Ko [9], the authors characterized driving performance based on drivers' steering behaviors to predict their gaze directions and inattention. A new image processing algorithm (e.g., Sobel operator) was presented, and the classification accuracy of the vigilance detection system exceeded 99%.

Vigilance is different from the concept of drowsiness, which refers to a person's tendency to fall asleep. Drowsiness impairs performance on attention-based tasks, leading to declined vigilance. Drowsiness often develops and varies on the scale of hours, whereas vigilance may change from minute to minute [9], [10]. In the current study, we used an operational definition of vigilance as measured by the RT to a lead car's brake events. These are natural driving events imbedded in car-following scenarios, and timely reactions are directly related to driving safety.

Measurement of driving performance is a straightforward method to monitor driver vigilance; however, there are still technological challenges regarding how to reliably measure the time period from the onset of a road event to a driver's response. As a result, many studies have explored the use of physiological and behavioral signals from the driver that can be recorded for vigilance monitoring and estimation. The major measures include eye and facial movements, blood pressure, cardiac and respiratory frequencies, hand trembling, galvanic skin resistance, heart rate variability, body temperature, oxygen concentration, and brain activities [3], [5], [7], [11]–[15]. Bergasa *et al.* [5] developed a nonintrusive prototype computer vision system to monitor six measures driver of vigilance in real time, including percent eye closure, eye closure duration, blink frequency, nodding frequency, face position, and fixed gaze. The system was verified in a real vehicle experiment, in which the driver's vigilance level was predicted using a fuzzy classifier with an overall accuracy of approximately 95%.

Giusti *et al.* [15] designed an intelligent system to detect a driver's vigilance level based on physiological data (e.g., cardiac and respiratory frequencies and galvanic skin resistance) acquired from sensors on the steering wheel. A simulated driving task was conducted with a mechanical platform whose data were also acquired. Based on fuzzy classification, a controller that monitored the number of heartbeats and the steering-wheel position was implemented to determine a high risk and alert the driver.

Lin *et al.* [3] presented a wireless EEG system [16] to monitor a driver's vigilance status in real time. The RTs to lane departure events were measured to indicate different levels of vigilance. The proposed system processed EEG recordings and predicted vigilance levels. A case study involving 15 participants assigned a 90-min sustained-attention driving task in a simulated driving environment demonstrated the reliability of the proposed system. Power spectral analysis results confirmed that the EEG activity correlated well with variations in vigilance. The PSD of alpha, beta, and the frequency bands at 10 Hz were the most sensitive indices for vigilance detection.

Recently, new wireless headsets (e.g., Emotiv) have become more cost effective, easier to use, and mobile, with increased practicability and fewer physical restrictions. An EEG has distinct advantages in practical usage and, therefore, has been a primary option for the development of online driver vigilance detection systems. In fact, there has been a growing amount of effort to recognize a driver's vigilance level in real time from EEG signals [3], [7]. Compared to other physiological signals, EEGs are highly sensitive to changes of vigilance states [17]–[19]. The alpha (8–12 Hz) and beta (13–30 Hz) rhythm components have a close relationship to the driver's vigilance level [20], [21]. Previous studies showed that the PSDs in the posterior brain region were stable and effective features for estimating the driver's vigilance states [22], [23]. Based on the PSD features of the EEG, various feature extraction (e.g., FFT and discrete wavelet transform), and feature selection algorithms (e.g., principal component analysis and linear discriminant analysis), as well as machine learning techniques (e.g., SVM, artificial neural network, and fuzzy expert system) have been compared to better predict a driver's vigilance state [6], [24]–[28].

The existing driver vigilance detection systems relied on physiological signals or driving behaviors, but ignored the impacts of driving contexts on a driver's vigilance. The objective of the current study is to propose a driver vigilance detection system through the analysis of not only brain activities but also driving context related factors, with a focus on vigilance prediction on a time scale of seconds. The results of a simulated driving experiment indicated that adding a newly driving context factor, road curves, could improve the prediction accuracy by 2–5% with 30–80 ms smaller errors.

The remainder of this paper is organized as follows. In Section II, the impacts of driving contexts on a driver's vigilance are introduced. In Section III, the general architecture of the proposed driver vigilance detection system is presented. In Section IV, the design of a simulated driving experiment is described, and validation results are provided. Finally, a discussion and conclusion are presented in Section V.

II. Impact of Driving-Context-Related Factors on the Detection of Driver Vigilance

Existing driver vigilance detection systems have been proposed and validated for relatively simple and monotonous driving tasks. Under well-controlled laboratory conditions, a driver's ability to sustain attention or vigilance level is exclusively affected by these simple and monotonous driving tasks. A driver's performance-related measures (e.g., the RT to natural driving events imbedded in lane-changing or car-following scenarios) are used to indicate various levels of driver vigilance. All conclusions are drawn on the basis of an assumption: a slower RT indicates a lower vigilance level. However, this assumption may not be valid in real driving scenarios.

The reliability of existing driver vigilance detection systems faces great challenges in practice. The input data collected from drivers, including behavioral and physiological signals, are insufficient to recognize a driver's vigilance state. The reason is that many tasks in real driving scenarios require a driver's sustained attention [29], [30]. For example, driving on curves usually requires a driver to judge how sharp the curve is, slow down before entering the curve, look for signs indicating curves, look ahead to identify the sharp turns ahead, and try to predict the length and approximate angle of the curve to know how to prepare for a better and smoother maneuver [31]. In this case, a driver's RTs to lane departure events or a lead car's brake events will be influenced. A driver may assign part of his attention to the lane maneuvering task, depending on how sharp the curve is and on his driving skill and experience [32]. Therefore, the predicted decrease of driver vigilance may result from the demands of lane maneuvering. In other words, driving straight or on curves contributes to the prediction accuracy of driver vigilance level and must be considered as inputs to the existing driver vigilance detection systems.

To improve the reliability of the existing driver vigilance detection systems, more driving-context-related variables should be taken into consideration to make more accurate predictions and warnings [33]. Here, the driving context is what surrounds a vehicle, and in driverless and autonomous driving, the term is primarily used in reference to the physical context that surrounds the operation of a vehicle [34]. Driving context variables can be divided into two categories: environmental and vehicle-related variables. Distinct from behavioral and physiological signals collected from drivers, environmental and vehicle-related variables are primarily recorded from the surrounding environment via one or multiple cameras, a global position system, and in-vehicle devices.

The first category refers to environmental and roadway-related factors that may influence drivers' engagements in driving activities, such as posted speed limits, curves, roadway traffic flow, road signs, weather, signal lights, etc. Similar to driving on curves, driving at higher speed gives a driver less time to react in an emergency. This may increase the driver's sustained attention and the allocation of mental resources, leading to a higher vigilance level but longer RTs to lane departure events. Driving freely (i.e., in a lower traffic density) may lead to more use of the cruise control. When reacting to a lane departure event, the driver must cancel the state of cruise control first and then take the evasive actions [35]. In these cases, the driver should be provided an early warning or other feedback if his predicted vigilance level is below a threshold [36].

The second category refers to vehicle-related factors that may distract drivers' attention from driving activities, such as the use of a radio, a global position system, a cell phone, etc. For example, the use of a cell phone while driving engages a driver to be less attentive to safety signals [37]. In such a dual-task (driving and use of cell phone) driving condition, how to define and measure driver performance to indicate driver vigilance states is challenging in practical driving scenarios.

III. Driver Vigilance Detection System Architecture

The general architecture of our proposed driver detection system is shown in Fig. 1; it includes five major components: an EEG and driving behavioral data acquisition, driving context awareness, EEG signal preprocessing and feature extraction, a driver vigilance classification and prediction model, and a driver feedback system with warning control strategy.

A. Data Acquisition

We used a 64-channel Neuroscan-SynAmps2 system to record EEG signals when the driver operated the driving simulator. The 64 active electrodes were attached to an electrode cap, which was convenient for us to select appropriate brain regions. We focused on the posterior brain region, which is sensitive to a driver's vigilance state. Seven channels (P1, P2, P3, P4, P5, P6, and P7) from this brain region were used. To set up a real-time system prototype, we connected to a Neuroscan acquisition server via TCP/IP to read the EEG data stream and then loaded the EEG data into EEGLAB, an open-source MATLAB toolbox for physiological signal processing [38]. EEGLAB provides various algorithms to process the EEG data, extract the PSD features, and recognize the driver's vigilance state.

Driving behaviors, such as speed, steering wheel angle, lane position, throttle, and brake pedal positions, were automatically recorded, synchronized, and sent to another computer using a serial communications port. The sampling rate of driving behavioral data was 50 Hz. In order to record a driver's RTs to driving events/stimuli with the minimum interference from EMG signals, we asked the driver to press a button when a lead car suddenly brakes. RTs were calculated from the onset of the brake lights of a lead car to a driver's button press.

B. Driving Context Awareness

A driving-context-aware system gathers information about the environment and vehicle. Sensors are mainly video cameras.

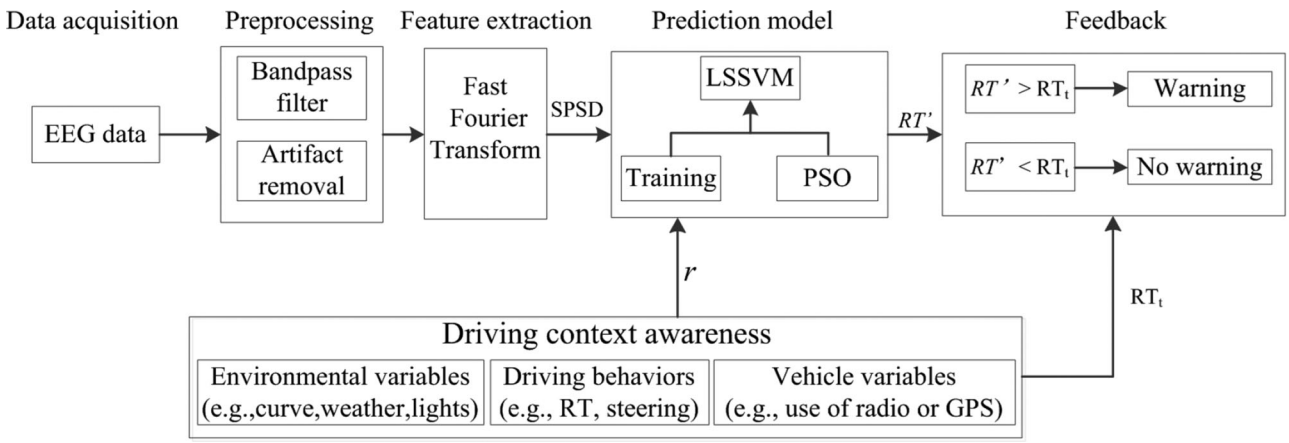

Fig. 1. Flowchart of the proposed driver vigilance detection system.

Image or video data are recorded in the vehicle and analyzed for improved traffic safety or comfort. Vision-based technologies are the general disciplines for designing solutions for the understanding of not only road curves, road signs, and vehicle flow [39]–[41], but also a driver's in-vehicle activities that distract his attention from the primary driving tasks [42], [43]. These environmental and vehicle related signals are recorded, fused, analyzed, and interpreted to create a driving context. Driving context and EEG features are then fed into a machine learning system from which a probability-based prediction of driver vigilance level is deduced. In our simulated driving experiment, road curves were predesigned and we controlled the other driving context variables at the same levels to investigate the potential effect of curves on the prediction accuracy of driver vigilance states.

C. EEG Signal Preprocessing and Feature Extraction

To achieve a better performance, we preprocessed the data by removing artifacts in the process of EEG recording to maintain signal stability and retain the effective data segments. First, continuous EEG data were filtered with a bandpass (0.1–30 Hz) filter to remove linear trends and minimize the introduction of artifacts. Second, we performed ICA to decompose the entire training dataset of EEG signals into independent components, which were characterized by their topographies and PSDs. Visual inspection and ratings by two experts marked each independent component as either an EOG or an EMG artifact or EEG signal component. The components marked as artifacts were discarded from the subsequent process. The remaining ones, classified as signal components, were back projected to reconstruct artifact-free EEG signals [44], [45]. Third, we rereferenced the data to the average of the two electrodes. Finally, we went through the whole dataset for each participant and blocked off all sections of data that were contaminated.

To recognize a driver's continuous vigilance states, we used an STFT with a sliding time window approach for feature extraction. The STFT is based on time–frequency analysis, which represents the EEG signals in a 2-D spectral domain and provides insights into both the frequency and temporal evolution of the energy- and power-related features that are associated with brain activities [45]. It is a linear decomposition of the EEG signals into elementary components. The STFT involves a sliding window of the EEG signal $x(m)$ around a time instant *t* from an experimental trial and the subsequent calculation of the Fourier transform for each *t*

$$X(t,f) = \int_{-\infty}^{\infty} w\,(m-t)\,x\,(m)\,e^{-\mathrm{j}2\pi\,\mathrm{fm}}\,dm \tag{1}$$

where $w(m-t)$ represents the short-time analysis window, and $X(t,\omega)$ represents the power distribution of the signal in the time–frequency plane. In essence, the STFT extracts several frames of the signal to be analyzed by using a window that moves with time. Each frame that is extracted is viewed as stationary, which enables the FFT to be used. By moving the window along the time axis, the relation between the variance of the frequency and time can be identified.

As illustrated in Fig. 2, a 3-s EEG epoch before each driving event (i.e., brake lights of a lead car) was split into four segments using a 1-s sliding time-window with a 50% overlap between two consecutive windows. We extended each 1-s segment to 512 points by zero padding and used a 512-point FFT to transform it to the frequency domain, resulting in PSD estimation with a frequency resolution of approximately 1 Hz. The PSDs of alpha (8–12 Hz) and beta (13–30 Hz) bands were computed, and there were 14 PSD features (2 frequency bands $\times$ 7 channels) for each 3-s epoch.

Because the fluctuation of vigilance with cycle length is typically more than 4 min [46], in the current study, eight consecutive 3-s epochs (epo1–epo8 in Fig. 2) were used to predict a driver's RT to the epo1's brake light event. A weighted-averaging filter was applied to obtain smoother PSD estimates [3]. SPSD denotes the smoother PSD estimate, m denotes the mth trial, and w_i is the weight of the PSD of the ith epoch. Because PSD features extracted from epo1 were more accurate to predict a driver's RT to the epo1's brake light event than those estimates from epo8, we assigned a higher weight to w_1 than w_8, i.e., $w = [8,7,6,5,4,3,2,1]$

$$\mathrm{SPSD}(m) = \frac{1}{8}\sum_{i=1}^{8}\mathrm{PSD}_i \cdot w_i. \tag{2}$$

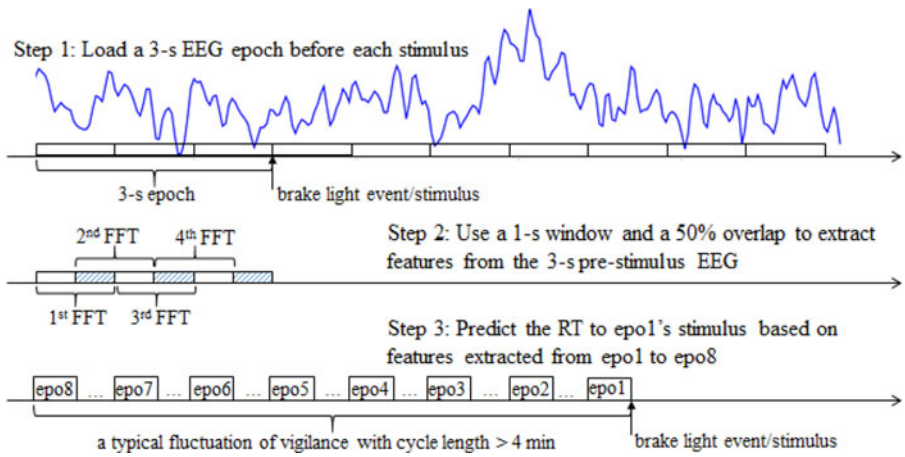

Fig. 2. Three-second EEG epoch before each event was loaded. Then, a 1-s window with a 50% overlap between two consecutive windows was used to segment the EEG data. PSD features were computed in each 1-s window, and eight consecutive epochs (epo1–epo8) were used to predict a driver's RT to the epo1's brake light event/stimulus.

In addition, road condition was also a driving context variable in the current study. We used r to denote the absence/presence of curves; $r = 1$ means the brake light stimulus occurred on a curved road, and $r = 0$ means the road was straight.

The EEG and driving context feature vectors X were formed as $X = \{[\mathrm{SPSD}(m), r(m)] | \mathrm{SPSD}(m) \in R^{14\times M}, r(m) \in R^{1\times M}\}$. The goal vectors $Y = \{y(m) | y(m) \in R^{1\times M}\}$ were the RTs; M was the total number of analyzed trials.

D. Driver Vigilance Classification and Prediction Model

According to the literature, the relationship between the PSD and RT is nonlinear. The SVM and SVR have been widely used to construct nonlinear models. The goal of SVR is to find the optimal hyperplane in the space, and the optimal hyperplane of the SVR predicts the distribution of data. Given the training data, if SVR is able to find a function $f(x_i) = \omega_i \cdot x_i + b, i = [1, 2 \ldots, l]$ that has a small difference between $f(x)$ and y for all training samples, the function $f(x)$ can predict y, and ω is the optimal hyperplane. The SVR can be formulated as follows:

$$\text{minimize } \frac{1}{2}\|\omega\|^2 + C\sum_{i=1}^{l}(\xi_i + \xi_i^*)$$
$$\text{subject to } \begin{cases} y_i - \omega \cdot x_i - b \le \varepsilon + \xi_i \\ \omega \cdot x_i + b - y_i \le \varepsilon + \xi_i^* \\ \xi_i, \xi_i^* \ge 0. \end{cases} \tag{3}$$

Here, ξ_i and ξ_i^* are slack variables for each training instance; slack variables determine whether this training instance can fall outside the range of ε. The constant C is used to adjust the training model to avoid overfitting or underfitting.

To better solve the nonlinear problem, in this study, we used the RBF to cross the linear threshold

$$k(x_i, x_j) = \exp\left(\frac{\|x_i - x_j\|}{2\sigma^2}\right) \tag{4}$$

where σ determines the width of the RBF kernel function.

The LSSVM, original from the standard SVM, converts the time-consuming quadratic programming problem into solving a system of linear equations, which effectively reduces the complexity of calculation and accelerates the operational speed. The main idea of the LSSVM is that it translates solving the problem of nonlinear regression in a lower dimensional space into solving the problem of linear regression in a high-dimensional space. For the same training data of SVR, the function of linear regression is defined as follows:

$$f(X) = W^T\phi(X) + d. \tag{5}$$

Here, W is the weight vector, d is the bias, and $\phi(\cdot)$ is the mapping to the high-dimensional feature space. The optimization problem of regression is formulated according to the regularized risk minimization principle. The final solution of the primal problem can be expressed as follows:

$$f(x) = \sum_{i=1}^{l}\alpha_i K(x, x_i) + d. \tag{6}$$

Here, α is the Lagrange multiplier. The kernel function $k(\cdot)$ is the same as (4).

The parameters C and σ for SVR and the parameters γ and σ for LSSVM are the key factors for these two models; PSO was used to find the best solutions for them. The PSO algorithm was inspired by social behaviors of bird flocking and has been widely applied in machine learning. In PSO, each particle moves through the search space with a velocity vector that is dynamically adjusted according to the particle's own fitness and the whole particle group's best solution fitness achieved so far. Optimization is terminated when a preset maximum iteration number is reached or the fitness threshold is met.

As shown in Fig. 3, all particles in PSO are directed with some randomness toward the area that contains the best solutions identified by the whole particle group. Taking optimizing SVR as an example, the best solution of SVR in the virtual search space was realized though a swarm of particles searching for the position (C, σ). During each generation, each particle's moves

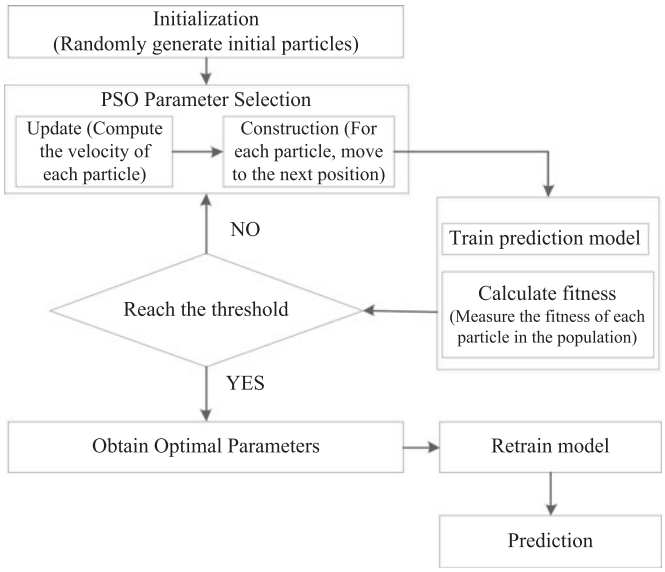

Fig. 3. Optimization process of PSO.

should be restricted by its individual best position and the best global position. The moving process of a particle is described as

$$\upsilon_{n,d}^{t+1} = \varpi^t \upsilon_{n,d}^t + c_1 \cdot r_1 \cdot (P_{l\text{best}}^t - p_{n,d}^t) + c_2 \cdot r_2 \cdot (P_{g\text{best}}^t - p_{n,d}^t) p_{n,d}^{t+1} = p_{n,d}^t + \alpha \upsilon_{n,d}^{t+1} \quad (7)$$

where t denotes the tth generation, c_1 and c_2 are learning factors, $\upsilon_{n,d}$ is the velocity of particle n in dimension d, $P_{n,d}$ is the position of the particle n in dimension d, $P_{l\text{best}}$ represents the individual best position of particle, $P_{g\text{best}}$ is the best of all individual best positions of all particles within the swarm, r_1 and r_2 are normally distributed positive random numbers between 0 and 1, α is the constraint factor of velocity, and ϖ denotes the inertial weight coefficient.

The prediction models are trained for each participant individually. To find a more accurate prediction model with a small training data size, a three-fold cross-validation method was used to enhance the accuracy of the model. As EEG features are time dependent, the normal cross-validation method by selecting training data randomly for independent identical distributed data sets is not suitable and will lead to large overfitting when the adjacent (dependent) EEG features in the time domain are divided into both the training set and validation set [23]. As a result, each participant's training set is equally divided into three segments in chronological order, which can reduce the time-dependent influence of the EEG features and control overfitting.

E. Driver Feedback System

R^2 and the RMSE are two frequently used indices for evaluating model performance. R^2 results indicate how well the experimental data can be explained by the model. The RMSE measures the differences between model predictions and the values actually observed.

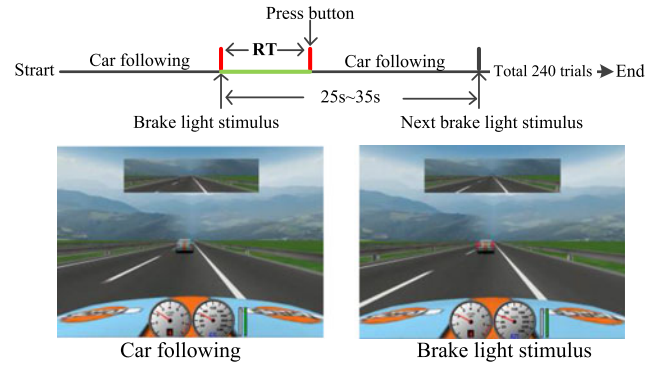

Fig. 4. Driving simulator and driving scenarios.

The warning message was scheduled and presented via an in-vehicle human–machine interface. When a driver's predicted vigilance level was below the predefined threshold, the system warned the driver visually and verbally. The visual information about the predicted vigilance state might be shown on an in-vehicle device (e.g., a global position system display) that increases in size and starts flashing. The verbal message such as "please pay attention to the driving task" can be repeated every 10 s until the driver's vigilance level returns to its normal state.

In addition, previous studies show that the acceptance of in-vehicle intelligent systems significantly increases with a higher warning threshold and lower warning frequency; however, the effects on driving behavior decrease [47]. This indicates that finding a balance between the acceptance and effectiveness of the system is quite crucial. Accordingly, the proposed system developed in this paper allowed the driver to customize the threshold for warnings and warning messages (e.g., tones or voice recordings from his family members) to increase system acceptance.

IV. Experimental Design and Results

A. Driving Simulator and Tasks

The experiment was conducted using a driving simulator consisting of a seat, a Logitech Driving Force G27 steering wheel, three pedals (throttle, brake, and clutch) and modified open-source software, "the open racing car simulator." A customized 1-bit USB key was used to record the participants' responses to the brake light stimulus/event. A projector and a 100-in screen with a resolution of 1024 × 768 and a refresh rate of 60 Hz were used to present the experimental task.

As illustrated in Fig. 4, the simulated driving scenarios consisted of a two-lane highway with both straight and curved segments. Traffic included the participant's vehicle and a lead vehicle. Participants were instructed to follow the lead vehicle while maintaining a safe distance but not to change lanes or overtake the lead vehicle. The speed of the lead vehicle varied randomly from 55 to 65 km/h. The lead vehicle was programmed to brake occasionally, and participants could see its brake lights illuminated. In each brake light event, participants were instructed to press the key as quickly as possible when they observed the

brake lights. There were a total of 240 brake light events, with a random interval of 25–35 s between two consecutive events.

As introduced in Section III-C, a typical cycle length of vigilance is more than 4 min. Therefore, we used eight consecutive brake light events ($30 \times 8 = 240$ s) to predict a driver's RTs to the current (e.g., epo1 in Fig. 2) brake light stimulus. These settings resulted in eight consecutive 3-s epochs (e.g., epo1–epo8 in Fig. 2), and 14 PSD features (2 frequency bands $\times$ 7 channels) were computed for each 3-s epoch. Because of the transition from the resting period to the simulated driving task, we excluded the data in the first 90 s (i.e., the first three brake light events) from the further analysis. The first prediction of a driver's RT was made for his response to the 11th brake light stimulus, and the M in Section III-C was set to 230.

B. Participants

A total of 20 legally licensed drivers (ages ranging from 22 to 27, mean $= 24.3$, SD $= 2.4$ years) took part in this study. All participants had normal or corrected-to-normal vision and had at least 5000 km of driving experience. None of them had any history of neurological or psychiatric illness or the need for any medications or other forms of drugs that might influence the central nervous system. All participants were asked to avoid drinking alcohol, coffee, or energy drinks two days before the experiment and refrain from eating or exercising 2 h before the experiment.

C. Experimental Procedure

To obtain more obvious changes of vigilance states, all experiments started at 2 P.M. After the setup of the EEG electrodes, participants were instructed to practice for approximately 15 min and get familiar with the driving simulator. In the formal experiment, they were required to drive for 2 h, simulating a prolonged driving scenario on the highway.

Impedances of all electrodes were kept below 5 kΩ. The EEG from each electrode site was digitized at 500 Hz with an amplifier bandpass of 0.5–100 Hz, and electrodes were arranged based on the extended 10/20 system with a reference on the top of the scalp. M1 was used as an online reference for all channels.

D. Experimental Results

1) Relationship Between RT and Road Conditions: The average RT of 20 participants to the brake light stimulus was 1029.9 ms (SD $= 148.5$) while driving on the straight road, increasing to 1076.1 ms (SD $= 143$) when the stimulus appeared on a curved road. The result of a paired *t*-test shows that the RT to the stimulus while driving on a curved road was significantly longer than that in a straightaway ($t(19) = -7.349, p < 0.01$). This result indicated that compared to a straight road, a curve may increase a driver's sustained attention to the demands of lane maneuvering. The allocation of the attention resource changed: the resource that was allocated to detecting the brake light stimulus diminished, leading to the lapse of driver vigilance in terms of the increased RTs. This finding suggested that road condition (i.e., the presence of a curve) served as an effective driving context feature that contributed to system performance.

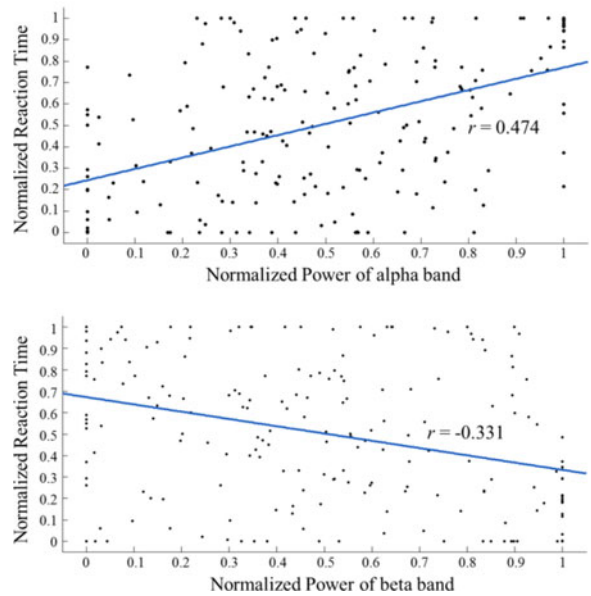

Fig. 5. Normalized RT changes across the normalized alpha (upper) and beta (lower) power bands.

TABLE I
COMPARISONS OF PERFORMANCE FOR DIFFERENT CLASSIFICATION MODELS (MEANS AND STANDARD DEVIATIONS)

Inputs	Model	Optimization method	R^2	RMSE(ms)
EEG features	SVR	PSO	0.816 (0.070)	188.20 (45.11)
		Grid-search	0.601 (0.129)	387.12 (224.32)
	LSSVM	PSO	0.828 (0.061)	191.19 (88.71)
		Grid-search	0.682 (0.17)	343.57 (198.43)
EEG features and driving context	SVR	PSO	0.837 (0.051)	165.52 (44.71)
		Grid-search	0.651 (0.155)	303.60 (211.87)
	LSSVM	PSO	0.841 (0.049)	162.21 (70.76)
		Grid-search	0.681 (0.131)	289.92 (224.18)

2) Relationship Between RT and PSD: Each participant's RTs and the corresponding powers of the alpha and beta bands were calculated and averaged. Due to large individual differences, all participants' RTs and PSDs were normalized into [0, 1]. As shown in Fig. 5, there was a positive correlation between the normalized RT and the normalized power of the alpha band ($r = 0.474$), and a negative correlation between the normalized RT and the normalized power of the beta band ($r = -0.331$). We further compared two vigilance states in terms of participants' performance: the best 25% of RTs (i.e., RTs < 800 ms, alert state) versus the worst 25% of RTs (RTs > 1500 ms, diminished vigilance state). We found that the mean power of the alpha band increased from 8.3 to 9.8 dB during the trials of long RTs, while the mean power of the beta band decreased from 8.1 to 6.2 dB at the same time. These results

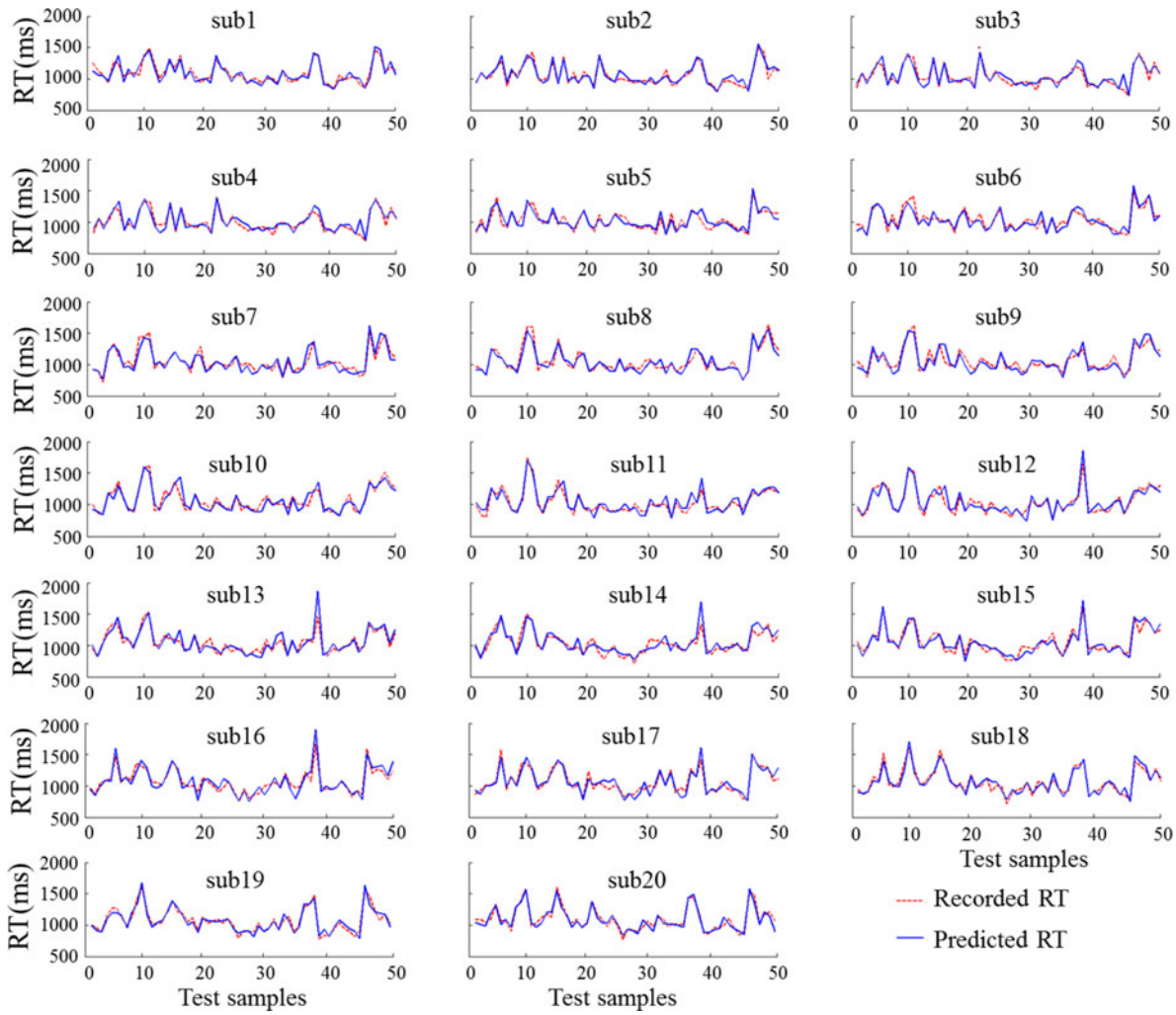

Fig. 6. Performance of the LSSVM-PSO model. Twenty participants' predicted and experimental RTs (50 samples) are presented from top to bottom and from left to right.

indicated the potential value of the PSD features of the EEG for predicting a driver's RT and vigilance states.

3) System Performance: To avoid the impact of individual differences of EEG signals on the system performance, all classification models were developed individually for the 20 participants. The PSD features extracted from the alpha and beta bands and road condition were used as inputs of the models. The RTs to the brake light stimulus was the goal of the models. Two widely used prediction models, SVR and LSSVM, were used predict the RT, and both models were constructed with the RBF kernel function. A threefold cross-validation method was performed. The optimized algorithm grid-search and PSO were compared to find the best solution. One hundred and eighty samples were used for a training model and the remaining 50 samples were test data. The R^2 and RMSE between the predicted RTs and experimental RTs were used to evaluate the performance of the models (means and standard deviations of models' performance are presented in Table I).

Three major conclusions were drawn from the results in Table I. First, the PSO outperformed the grid-search optimization algorithm regardless of the SVR or LSSVM model. The classification model with the PSO optimization algorithm was able to explain 14.6–21.5% more experimental RTs with 127.71–198.92 ms smaller prediction errors compared to the model with the grid-search method. The differences of system performance between the PSO and grid-search optimization algorithm were more evident when the PSD features served as the single inputs of the SVR model.

Second, the LSSVM outperformed the SVR. The LSSVM model with a grid-search optimization algorithm was able to account for 3–8.1% more experimental RTs with 13.68–43.55 ms smaller prediction errors than the SVR model with the same optimization method. However, such differences in the system performance between two classification models did not exist when the POS optimization method was used.

Finally, the feature vectors consisting of both the PSD and road condition enhanced the system performance. More specifically, when both feature vectors entered as model inputs, the driver vigilance detection system was able to account for, at most, 5% experimental RTs with 22.68–83.52 ms smaller prediction errors compared to the model with the single PSD features. These results confirmed our expectation that the road

TABLE II
PERFORMANCE OF LSSVM-PSO FOR 20 PARTICIPANTS

Participant number	R^2	RMSE (ms)	Participant number	R^2	RMSE (ms)
1	0.87	115.42	11	0.85	131.84
2	0.89	101.04	12	0.85	163.15
3	0.84	177.34	13	0.83	130.77
4	0.78	250.94	14	0.79	314.09
5	0.77	311.12	15	0.89	106.22
6	0.83	227.56	16	0.88	106.78
7	0.85	160.64	17	0.86	223.01
8	0.87	101.36	18	0.91	98.73
9	0.84	145.30	19	0.92	104.55
10	0.83	197.52	20	0.91	77.45

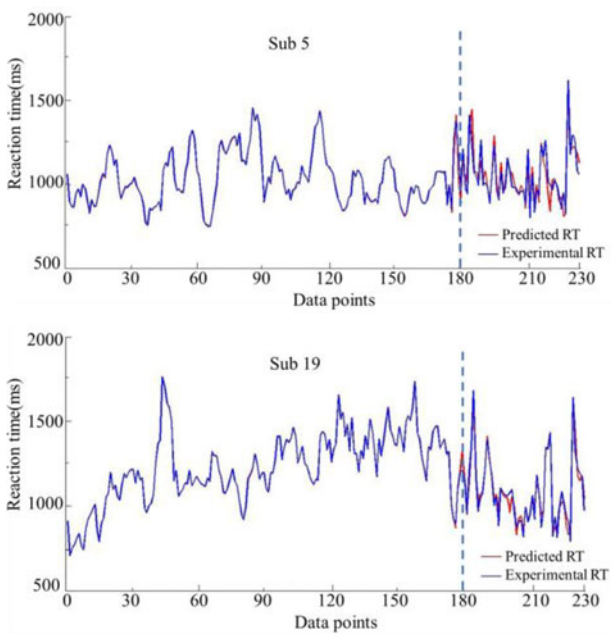

Fig. 7. Whole trials (230 samples) for the drivers with the worst (Driver 5, upper panel) and best (Driver 19, lower panel) prediction performance.

condition can be considered to be an important predictor of a driver's vigilance state that improves the reliability of the driver vigilance detection system. Overall, when the feature vectors consisting of both the PSD and the road condition served as inputs of the LSSVM PSO optimization algorithm (i.e., LSSVM-PSO), the proposed system achieved the best performance (highlighted with gray fill). It was able to account for 84.1% of experimental RTs with 162-ms prediction errors. Fig. 6 showed the performance of the LSSVM-PSO model. The LSSVM-PSO model predictions (red line) and experimental RTs (blue line) were presented, respectively. It is obvious that RTs to the brake light stimulus were significantly different across participants (see Table II). One participant (number 20) yielded one of highest R^2 (0.91) and the smallest RMSEs (77.45), compared to the lowest R^2 (0.77) and one of the highest RMSE (311.12). The whole trials for the drivers with the best and worst prediction performance were shown in Fig. 7. These findings suggested that we would better develop a customized LSSVM-PSO model for each driver to better predict his diminished vigilance state. On the other hand, for safety, a minimum reaction distance between vehicles of 20 m is recommended when driving at a speed of 100 km/h [3]. In this work, the majority of the errors between predicted and experimental RTs were less than 200 ms (approximately 5.5 m at 100 km/hr), which did not violate the recommended reaction distance.

V. DISCUSSION AND CONCLUSION

We have developed a classification model combining the LSSVM and PSO optimization algorithms to classify a driver's vigilance levels based on his brain activities and road conditions on a time-scale of seconds. Data were collected from a simulated driving experiment involving 20 drivers. In car-following scenarios, driver vigilance was operationally measured as the RT to the lead car's brake events. Our system was able to account for 84.1% of experimental RTs with 162-ms prediction errors. These findings demonstrate the potential value of the proposed system for estimating a driver's vigilance level in real time.

A newly introduced driving context factor, road curves, improved the prediction accuracy by 2–5% with 30–80 ms smaller errors. This finding indicated that a driver's RTs to a lead car's brake stimulus were influenced by the presence of a road curve. Driving straight or on curves contributed to the prediction accuracy of a driver's vigilance level. One possible explanation is that the car-following task competes with the lane-maneuvering task and both driving tasks consume a driver's attentional and cognitive resources, moderated by the driver's personal driving skill and experience. Therefore, the predicted decrease of driver vigilance results from the demands of not only car following but also lane maneuvering. Roadway curves should be considered as inputs to the existing driver vigilance detection systems.

In previous studies, Lin *et al.* [3] developed a system that processed EEG signals to predict a driver's vigilance levels. When the PSDs of delta (0–4 Hz), theta (4–8 Hz), alpha, and beta bands were entered into the SVR model as inputs, their system achieved an overall 81.6% classification accuracy with 207-ms prediction errors. Comparing this work, our LSSVM-PSO system, using the single PSD features of alpha and beta bands, was able to account for 82.8% of experimental RTs with 191.19-ms prediction errors, indicating a better performance. Of course, in [3], vigilance was measured as a driver's RTs to lane departure events, with fewer EEG electrodes in the posterior brain region; thus, performance differences may result from the differences in the experimental design and devices.

Because of the contribution of road curves to the recognition of a driver's vigilance state, further studies can continue to expand along this research line. First, in this study, road curves were regarded as a binary variable: the absence or presence of a curved road. Further studies may design different road curves with various radiuses of curvature and use these radiuses as the model inputs. Here, the assumption is that the larger the radius of curvature is, the more difficult the lane maneuvering task becomes, leading to more contribution of the lane maneuvering task to a driver's predicted RTs and vigilance levels.

In addition to road curves, other variables can be examined to validate the contribution of driving contexts to the system performance. For example, the following distance between a lead car and the following driver's vehicle may also affect the driver's RTs [48]. In the current study, the participants were instructed to maintain a safe distance to the lead car. Because we set the maximum following distance, the potential effect of the following distance on a driver's RTs should be tested in our further experiment. Road signs are another important category of driving contexts, such as the posted speed limit, stop/yield sign, traffic light, etc. A common feature of these road signs is that a driver has to respond immediately (e.g., slow down or fully stop at a signalized intersection) when they are perceived. As a result, the presence of road signs will compete with the primary car following task and leads to an increased RT to a road event. On the other hand, vehicle-related variables may distract a driver's attention from his primary driving activities, such as the use of a cell phone while driving. In such a dual-task (driving and use of cell phone) driving condition, how to measure and detect a driver's declined vigilance level or cognitive distraction (i.e., driving while thinking something unrelated to the primary driving task) is challenging in practical driving scenarios [49].

The current real-time system prototype should be validated in the real driving conditions, including the effectiveness and reliability of the proposed driver vigilance detection system as well as system acceptance with various warning strategies and modalities [47]. However, the application of feedback may result in a miss or a false alarm error, which must be taken into account. To solve this problem, the existing signal detection theory and model provide a powerful mathematical tool for the analysis and design of better warnings. It provides great insight on the manner that the presence or absence of a warning signal should be interpreted optimally [36]. For example, in order to define a personalized threshold to trigger a warning, we can set different thresholds and measure a driver's responses to the changes in the warning levels. The optimal warning system with the highest model sensitivity can be characterized by receiver operating characteristic curves.

ACKNOWLEDGMENT

The authors would like to thank the editor and reviewers for their valuable comments, which help improve the quality of this paper.

REFERENCES

[1] J. He *et al.*, "Texting while driving: Is speech-based text entry less risky than handheld text entry?" *Accident Anal. Prevention*, vol. 72, pp. 287–295, 2014.

[2] A. Campagne, T. Pebayle, and A. Muzet, "Correlation between driving errors and vigilance level: Influence of the driver's age," *Physiol. Behav.*, vol. 80, pp. 515–524, 2004.

[3] C. T. Lin *et al.*, "Wireless and wearable EEG system for evaluating driver vigilance," *IEEE Trans. Biomed. Circuits Syst.*, vol. 8, no. 2, pp. 165–176, Apr. 2014.

[4] W. Kong, W. Lin, F. Babiloni, S. Hu, and G. Borghini, "Investigating driver fatigue versus alertness using the granger causality network," *Sensors*, vol. 15, pp. 19181–19198, 2015.

[5] L. M. Bergasa, J. Nuevo, M. A. Sotelo, and M. Vazquez, "Real-time system for monitoring driver vigilance," *IEEE Trans. Intell. Transp. Syst.*, vol. 7, no. 1, pp. 63–77, Mar. 2006.

[6] C. T. Lin, K. C. Huang, C. H. Chuang, L. W. Ko, and T. P. Jung, "Can arousing feedback rectify lapses in driving? Prediction from EEG power spectra," *J. Neural Eng.*, vol. 10, Oct. 2013, Art. no. 056024.

[7] Z. Zhang *et al.*, "A vehicle active safety model: Vehicle speed control based on driver vigilance detection using wearable EEG and sparse representation," *Sensors*, vol. 16, Feb. 19, 2016, Art. no. 242.

[8] S. F. Zhao, G. Xu, and T. Tao, "Detecting of driver's drowsiness using multiwavelet packet energy spectrum," in *Proc. 2nd Int. Congr. Image Signal Process.*, Tianjin, China, 2009, pp. 1–5.

[9] J.-X. Liu and M.-K. Ko, "Detection of driver's low vigilance using vehicle steering information and facial inattention features," in *Proc. 20th ITS World Congr.*, Tokyo, Japan, 2013, pp. 2066–2075.

[10] T. P. Jung, S. Makeig, M. Stensmo, and T. J. Sejnowski, "Estimating alertness from the EEG power spectrum," *IEEE Trans. Biomed. Eng.*, vol. 44, no. 1, pp. 60–69, Jan. 1997.

[11] M. H. Sigari, M. Fathy, and M. Soryani, "A driver face monitoring system for fatigue and distraction detection," *Int. J. Veh. Technol.*, vol. 2013, pp. 73–100, 2013.

[12] Z. Zhang and J. Zhang, "A new real-time eye tracking based on nonlinear unscented Kalman filter for monitoring driver fatigue," *Control Theory Technol.*, vol. 8, pp. 181–188, 2010.

[13] B. G. Lee and W. Y. Chung, "Driver alertness monitoring using fusion of facial features and bio-signals," *IEEE Sens. J.*, vol. 12, no. 7, pp. 2416–2422, Jul. 2012.

[14] Q. Ji and X. Yang, "Real-time eye, gaze, and face pose tracking for monitoring driver vigilance," *Real-Time Imag.*, vol. 8, pp. 357–377, 2002.

[15] A. Giusti, C. Zocchi, and A. Rovetta, "A noninvasive system for evaluating driver vigilance level examining both physiological and mechanical data," *IEEE Trans. Intell. Transp. Syst.*, vol. 10, no. 1, pp. 127–134, Mar. 2009.

[16] C. T. Lin, C. H. Chuang, C. S. Huang, Y. H. Chen, and L. W. Ko, "Real-time assessment of vigilance level using an innovative Mindo4 wireless EEG system," in *Proc. IEEE Int. Symp. Circuits Syst.*, Beijing, China, 2013, pp. 1528–1531.

[17] S. Makeig and T. P. Jung, "Tonic, phasic, and transient EEG correlates of auditory awareness in drowsiness," *Cogn. Brain Res.*, vol. 4, pp. 15–25, 1996.

[18] C. T. Lin *et al.*, "Tonic and phasic EEG and behavioral changes induced by arousing feedback," *Neuroimage*, vol. 52, pp. 633–642, Aug. 15, 2010.

[19] S. K. Lal and A. Craig, "A critical review of the psychophysiology of driver fatigue," *Biol. Psychol.*, vol. 55, pp. 173–194, 2001.

[20] S. Makeig, T. P. Jung, and T. J. Sejnowski, "Awareness during drowsiness: Dynamics and electrophysiological correlates," *Can. J. Exp. Psychol.*, vol. 54, pp. 266–273, 2000.

[21] M. A. Schier, "Changes in EEG alpha power during simulated driving: a demonstration," *Int. J. Psychophysiol.*, vol. 37, pp. 155–162, 2000.

[22] C. T. Lin, C. H. Chuang, Y. K. Wang, S. F. Tsai, T. C. Chiu, and L. W. Ko, "Neurocognitive characteristics of the driver: A review on drowsiness, distraction, navigation, and motion sickness," *J. Neurosci. Neuroeng.*, vol. 1, pp. 61–81, 2012.

[23] L.-C. Shi and B.-L. Lu, "EEG-based vigilance estimation using extreme learning machines," *Neurocomputing*, vol. 102, pp. 135–143, 2013.

[24] C. H. Chuang, L. W. Ko, Y. P. Lin, T. P. Jung, and C. T. Lin, "Independent component ensemble of EEG for brain-computer interface," *IEEE Trans. Neural Syst. Rehabil. Eng.*, vol. 22, no. 2, pp. 230–238, Mar. 2014.

[25] S. W. Chuang, L. W. Ko, Y. P. Lin, R. S. Huang, T. P. Jung, and C. T. Lin, "Co-modulatory spectral changes in independent brain processes are correlated with task performance," *Neuroimage*, vol. 62, pp. 1469–1477, Sep. 2012.

[26] C. H. Chuang, Y. P. Lin, L. W. Ko, T. P. Jung, and C. T. Lin, "Automatic design for independent component analysis based brain-computer interfacing," in *Proc. 35th Annu. Int. Conf. IEEE Eng. Med. Biol. Soc.*, Osaka, Japan, 2013, pp. 2180–2183.

[27] I. G. Damousis, D. Tzovaras, and M. G. Strintzis, "A fuzzy expert system for the early warning of accidents due to driver hypo-vigilance," *Pers. Ubiquitous Comput.*, vol. 13, pp. 43–49, 2007.

[28] A. Yildiz, M. Akin, M. Poyraz, and G. Kirbas, "Application of adaptive neuro-fuzzy inference system for vigilance level estimation by using wavelet-entropy feature extraction," *Expert Syst. Appl.*, vol. 36, pp. 7390–7399, 2009.

[29] S. Cao, Y. Qin, X. Jin, L. Zhao, and M. Shen, "Effect of driving experience on collision avoidance braking: An experimental investigation and computational modelling," *Behav. Inf. Technol.*, vol. 33, pp. 929–940, 2014.

[30] S. Cao, Y. Qin, L. Zhao, and M. Shen, "Modeling the development of vehicle lateral control skills in a cognitive architecture," *Transp. Res. F, Traffic Psychol. Behav.*, vol. 32, pp. 1–10, 2015.
[31] T. Toroyan, "Global status report on road safety," *Injury Prevention*, vol. 15, pp. 286–286, 2009.
[32] S. L. Comte and A. H. Jamson, "Traditional and innovative speed-reducing measures for curves: An investigation of driver behaviour using a driving simulator," *Saf. Sci.*, vol. 36, pp. 137–150, 2000.
[33] C. Wu, O. Tsimhoni, and Y. Liu, "Development of an adaptive workload management system using the queueing network-model human processor (QN-MHP)," *IEEE Trans. Intell. Transp. Syst.*, vol. 9, no. 3, pp. 463–475, Sep. 2008.
[34] H. W. Gellersen, A. Schmidt, and M. Beigl, "Multi-sensor context-awareness in mobile devices and smart artifacts," *Mobile Netw. Appl.*, vol. 7, pp. 341–351, 2002.
[35] G. Zhao and C. Wu, "Mathematical modeling of driver speed control with individual differences," *IEEE Trans. Syst., Man, Cybern.: Syst.*, vol. 43, no. 5, pp. 1091–1104, Sep. 2013.
[36] G. Zhao, C. Wu, and C. Qiao, "A mathematical model for the prediction of speeding with its validation," *IEEE Trans. Intell. Transp. Syst.*, vol. 14, no. 2, pp. 828–836, Jun. 2013.
[37] D. L. Strayer and W. A. Johnston, "Driven to distraction: Dual-task studies of simulated driving and conversing on a cellular telephone," *Psychol. Sci.*, vol. 12, pp. 462–466, 2001.
[38] A. Delorme and S. Makeig, "EEGLAB: An open source toolbox for analysis of single-trial EEG dynamics including independent component analysis," *J. Neurosci. Methods*, vol. 134, pp. 9–21, 2004.
[39] M. Bertozzi and A. Broggi, "GOLD: A parallel real-time stereo vision system for generic obstacle and lane detection," *IEEE Trans. Image Process.*, vol. 7, no. 1, pp. 62–81, Jan. 1998.
[40] Y. He, H. Wang, and B. Zhang, "Color-based road detection in urban traffic scenes," *IEEE Trans. Intell. Transp. Syst.*, vol. 5, no. 4, pp. 309–318, Dec. 2004.
[41] G. Loy and N. Barnes, "Fast shape-based road sign detection for a driver assistance system," in *Proc. IEEE/RSJ Int. Conf. Intell. Robots Syst.*, Sendai, Japan, 2004, pp. 70–75.
[42] W. J. Horrey, M. F. Lesch, and A. Garabet, "Assessing the awareness of performance decrements in distracted drivers," *Accident Anal. Prevention*, vol. 40, pp. 675–682, 2008.
[43] J. Stutts *et al.*, "Driver's exposure to distractions in their natural driving environment," *Accident Anal. Prevention*, vol. 37, pp. 1093–1101, 2005.
[44] W. De Clercq, A. Vergult, B. Vanrumste, W. Van Paesschen, and S. Van Huffel, "Canonical correlation analysis applied to remove muscle artifacts from the electroencephalogram," *IEEE Trans. Biomed. Eng.*, vol. 53, no. 12, pp. 2583–2587, Nov. 2006.
[45] Y.-J. Liu, M. Yu, G. Zhao, J. Song, Y. Ge, and Y. Shi, "Real-time movie-induced discrete emotion recognition from EEG signals," *IEEE Trans. Affective Comput.*, to be published.
[46] S. Makeig and M. Inlow, "Lapse in alertness: coherence of fluctuations in performance and EEG spectrum," *Electroencephalogr. Clin. Neurophysiol.*, vol. 86, pp. 23–35, 1993.
[47] G. Zhao and C. Wu, "Effectiveness and acceptance of the intelligent speeding prediction system (ISPS)," *Accident Anal. Prevention*, vol. 52, pp. 19–28, 2013.
[48] G. Li, W. Wang, S. E. Li, B. Cheng, and P. Green, "Effectiveness of flashing brake and hazard systems in avoiding rear-end crashes," *Adv. Mech. Eng.*, vol. 6, 2014, Art. no. 792670.
[49] Y. Liao, S. E. Li, W. Wang, Y. Wang, G. Li, and B. Cheng, "Detection of driver cognitive distraction: A comparison study of stop-controlled intersection and speed-limited highway," *IEEE Trans. Intell. Transp. Syst.*, vol. 17, no. 6, pp. 1628–1637, Jun. 2016.

Zizheng Guo received the B.S. degree in railway transportation, the M.S. degree in traffic safety, and the Ph.D. degree in traffic planning and management from Southwest Jiaotong University, Chengdu, China, in 2003, 2005, and 2009, respectively.

He was a Postdoctoral Fellow at the Institute of Psychology, Chinese Academy of Sciences, during 2011–2013, and was a Visiting Scholar with the University of Michigan during 2013–2014. He is currently an Associate Professor with the Department of Transportation and Logistics, Southwest Jiaotong University.

Yufan Pan received the B.S. degree in electronic information engineering from the University of Electronic Science and Technology of China, Chengdu, China, in 2010. He is currently working toward the M.S. degree at the Institute of Transportation and Logistics, Southwest Jiaotong University, Chengdu.

His research interests include machine learning, traffic safety, and biomedical signal processing.

Guozhen Zhao received the B.S. degree in industrial engineering from Tianjin University, Tianjin, China, in 2007, and the M.S. and Ph.D. degrees in industrial and systems engineering from the State University of New York, Buffalo, NY, USA, in 2009 and 2011, respectively.

He is an Associate Professor at the Institute of Psychology, Chinese Academy of Sciences, Beijing, China. His current research interests include the mathematical modeling of human cognition and performance, human–computer interaction, emotion recognition, and augmented cognition.

Shi Cao received the Ph.D. degree in industrial and operations engineering from the University of Michigan, Ann Arbor, MI, USA, in 2013.

He is an Assistant Professor with the Department of Systems Design Engineering, University of Waterloo, Waterloo, ON, Canada. His research interests include human performance and workload modeling, transportation human factors, and human–computer interaction.

Jun Zhang received the B.S. degree in information science and technology and the M.S. degree in traffic planning and management from Southwest Jiaotong University, Chengdu, China, in 1998 and 2000, respectively.

His current research interests include the traffic safety, human–computer interaction, and railway safety.